Alvarez-Clemares, I.; Borrell Tomás, MA.; Agouram, S.; Torrecillas, R.; Fernandez, A. (2013). Microstructure and mechanical effects of spark plasma sintering in alumina monolithic ceramics. Scripta Materialia. 68(8):603-606. doi:10.1016/j.scriptamat.2012.12.016.

Available online at www.sciencedirect.com

SciVerse ScienceDirect

Scripta Materialia 68 (2013) 603–606

Scripta MATERIALIA

www.elsevier.com/locate/scriptamat

Microstructure and mechanical effects of spark plasma sintering in alumina monolithic ceramics

I. Álvarez-Clemares,[a] A. Borrell,[b,*] S. Agouram,[c] R. Torrecillas[a] and A. Fernández[a,d]

[a]*Centro de Investigación en Nanomateriales y Nanotecnología (CINN) (Consejo Superior de Investigaciones Científicas, Universidad de Oviedo, Principado de Asturias), Parque Tecnológico de Asturias, 33428 Llanera, Spain*

[b]*Instituto de Tecnología de Materiales, Universidad Politécnica de Valencia, Camino de Vera s/n, 46022 Valencia, Spain*

[c]*Departamento de Física Aplicada y Electromagnetismo, Universidad de Valencia, Dr. Moliner 50, 46100 Burjassot, Spain*

[d]*ITMA Materials Technology, Parque Tecnológico de Asturias, 33428 Llanera, Spain*

Received 8 November 2012; revised 6 December 2012; accepted 11 December 2012
Available online 20 December 2012

The specific effects of spark plasma sintering (SPS) on the creep behavior, microstructure and mechanical properties of alumina monolithic ceramic were investigated. SPS introduces strains that concentrate at grain boundaries and inhibit crack growth, resulting in an improvement in the flexural strength and fracture toughness. However, creep blocks grain boundary movements and decreases the reliability of the material. These strains can be removed by a post-sintering thermal treatment, which plays an important role in the distribution of dislocations.

Keywords: Transmission electron microscopy; Ceramics; Dislocations; High-temperature deformation; Mechanical properties

Since the first report by Wakai et al. [1,2] of superplastic flow in ceramic materials, significant advances in the development of superplastic ceramics have been made. Ceramics that have demonstrated superplasticity include single-phase systems such as yttria-stabilized tetragonal zirconia polycrystals (Y-TZP) [1], two-phase systems such as zirconia–mullite [3], Y-TZP with silica [4] and yttria cubic stabilized zirconia with silica additions [5]. More recently, three-phase systems such as alumina–spinel TZP [6] and alumina–mullite ($3Al_2O_3 \cdot 2SiO_2$)–TZP [7] have shown high strain rate potential. The key to superplastic deformation in all of these systems is the fabrication of a material with a fine grain size (usually <1 μm for ceramics) and limited grain growth upon high-temperature deformation [8].

Spark plasma sintering (SPS) makes it possible to sinter nanometric powders with near-theoretical values of density and little grain growth (<1 μm). This technique can work at heating rates of hundreds degrees per minute, reaching high temperatures in a short time, and producing dense materials at comparatively low sintering temperatures, typically a few hundred degrees lower than in normal hot pressing or pressureless sintering [9–14]. These features can produce microstructures unattainable by other sintering techniques. It has also been reported that SPS materials show mechanical properties that differ from those of materials sintered by other methods [11,13,14]. Gao et al. [11] found that SPS alumina showed a flexural strength double that of the same material sintered under pressureless conditions. Tamari et al. [14] compared the properties of a titanium carbide whisker/alumina composite as a function of the sintering method (hot pressing and SPS) and reported that the mechanical properties of the SPS materials were slightly higher. Those studies attributed this improvement in the material features to the finer microstructure and higher density achieved with the SPS process. The present work, however, represents a totally different approach, demonstrating that SPS has a specific effect on the creep behavior of ceramics. This work attempts to investigate the microstructure in depth using high-resolution transmission electron microscopy (HR-TEM) morphology in order to further clarify the effects of SPS on the deformation mechanisms that exist at high temperatures in sintered alumina material.

The material used in this investigation is a commercial submicrometric α-alumina (Taimei TM-DAR Chemicals Co. Ltd., Japan) with an average particle size

* Corresponding author. Tel.: +34 963 877 007; fax: +34 963 877 629; e-mail: aborrell@upvnet.upv.es

1359-6462/$ - see front matter
http://dx.doi.org/10.1016/j.scriptamat.2012.12.016

of 153 nm and a purity of 99.99%. As-received powder was poured into a graphite die with an inner diameter of 20 mm and pre-pressed to 15 MPa before sintering. An SPS apparatus (HP D25/1, FCT Systeme GmbH) was used for sintering in vacuum at 1300 °C, 80 MPa (applied from 600 °C until the end of the process) and 2 min dwell time. The heating rate was 50 °C min^{-1} and the cooling rate about 400 °C min^{-1}. After sintering, some samples received a thermal treatment (annealing) that consisted of heating in air at 1000 °C for 5 h to eliminate the residual strains. The final density of the materials was determined by the Archimedes method and referred to the theoretical density of 3.98 g cm^{-3} for alumina.

To perform the mechanical tests of annealed and as-sintered alumina samples, the specimens were cut into $3 \times 4 \times 18$ mm parallelepipeds. The tensile face of all the specimens was polished with diamond paste down to 3 μm (Struers, RotoPol-31) and the edges were chamfered (~45°) in order to avoid the influence of microcracks on creep behavior.

The fracture toughness (K_{IC}) of both kinds of materials was calculated from the crack length of the indentation in the polished samples [15]. For that purpose, a Leco AMH43 macroindenter with a 98 N load was used.

The flexural strength at different temperatures was measured with a mechanical test machine (Instron Fast Track 8800, using Bluehill software) in a three-point-bending apparatus with an inner spam of 15 mm and a crosshead speed of 0.5 mm min^{-1}.

In order to study the effect that these strains have on the high-temperature deformation of the materials, creep behavior was measured by means of three-point bending tests, using the same machine and apparatus as in the case of flexural strength. The approximation proposed by Hollenberg et al. [16] was used to calculate the deformation and creep rate. The elongation was measured with a precision of 1 μm. The tests were performed at 1200 °C. To ensure the homogeneity of the temperature in the chamber the load (50 N) was applied after 1 h of soaking time at 1200 °C.

The morphology and microstructural characterization of the sintered bodies (annealed and non-annealed) were performed by TEM, HR-TEM and selected-area electron diffraction (SAED) by using a Tecnai G2 F20 field emission gun transmission electron microscope operated at 200 kV.

In order to study the crystalline properties and crystalline defects (e.g. dislocations) of alumina samples, a careful preparation procedure was followed: after standard mechanical polishing to a thickness of <150 μm a dimpling on both samples using a 3 mm diameter disc to a thickness in the center of the sample of about 30 μm was achieved. After that, an ion milling procedure was performed using a Fishione Model 1010 machine. As a first step, samples were milled at 5 kV and 20° milling angle; in order to avoid artefacts generated during milling at high energy, a low ion beam energy (3 kV) and low milling angle of 10° were then used to produce a large, thin and clean area for HR-TEM characterization.

The final densities of alumina materials (non-annealed and annealed) were 99.9% of the theoretical density. Therefore, this shows that the post-sintering heating treatment does not affect the density of the final material.

Table 1 lists the creep deformation and fracture toughness values for the fired specimens.

According to the results from creep tests at 1200 °C and 50 MPa, as-sintered alumina presented very low deformation (<0.1%) and creep rate. Nevertheless the sample broke at 40 h. The annealed sample presented a much higher deformation, reaching a deformation of 22.0% after 80 h without breaking. This fact can be explained if we consider that grain boundary sliding is the main high-temperature deformation mechanism of alumina. On the one hand, when the sample is sintered by SPS the dislocations induced by the sintering mechanisms block the grain boundary movement, leading to a very low deformation rate. However, in this case the material cannot accommodate the deformation produced and breaks. On the other hand, when the same material has been previously annealed the deformation rate in considerably higher and the material presented elongations up to 20% and as a consequence of that the material is more reliable.

Considering the fracture toughness, all samples present high values, ranging between about 3 and 5 MPa $m^{1/2}$; as expected, the higher K_{IC} values were determined for the non-annealed alumina. Therefore, the results confirm that the strains promoted by SPS act as crack propagation inhibitors, explaining the higher fracture toughness values obtained for SPS samples in this work and in other work reported in the literature [14].

The results of the flexural strength as a function of temperature for non-annealed and annealed alumina are plotted in Figure 1. It can be observed that the values obtained for the non-annealed sample are significantly higher in the temperature range 400–800 °C.

Table 1. Creep deformation and fracture toughness (K_{IC}) of the alumina sintered samples.

	Non-annealed alumina	Annealed alumina
Creep deformation (%)	1.4 ± 0.2	22.0 ± 0.4
Fracture toughness (MPa $m^{1/2}$)	4.3 ± 0.4	3.4 ± 0.1

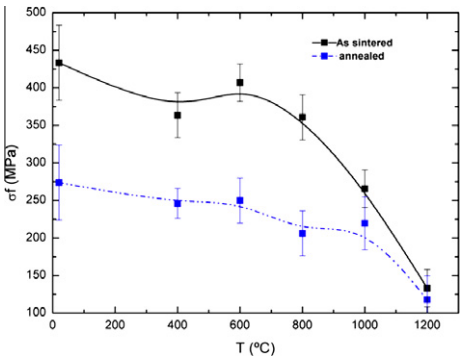

Figure 1. Flexural strength as function of temperature for non-annealed and annealed alumina.

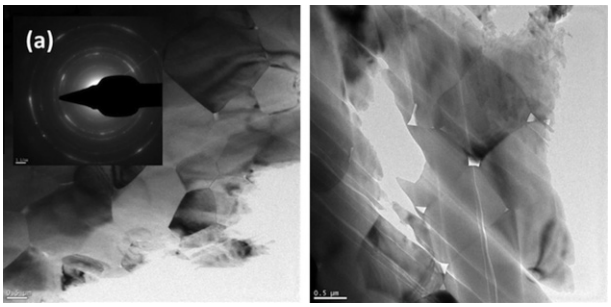

Figure 2. TEM micrographs of (a) non-annealed sample and (b) annealed sample. The inset figure represents the SAED of (a).

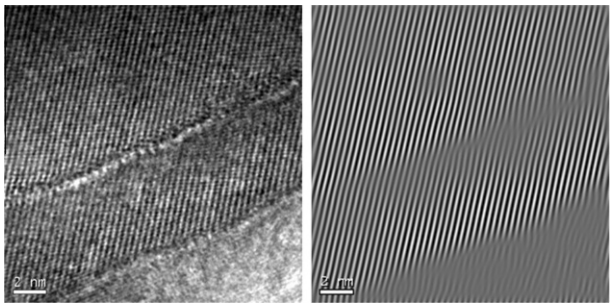

Figure 4. (a) HR-TEM and (b) Fourier-filtered images of a representative zone in sample 1.

Hence, the residual strains could have been activated in compression and thus inhibited crack growth. In addition, an increase in the flexural strength of materials with induced strains has been reported by Kirchner and Gruver [17]. Values for temperatures higher than 1000 °C are almost the same for both materials; this is completely logical because this temperature corresponds to the one used for the annealing treatment, and thus the residual strains in both materials have been relaxed.

Direct observation of the grain boundaries and morphologies of the microstructures were achieved by TEM and HR-TEM. Figure 2 shows representative TEM micrographs of samples 1 and 2 (non-annealed and annealed, respectively): in both samples we observe that the sample consists of large grains with sizes ranging from 500 nm to 2 μm. The TEM images demonstrate the augmentation of grain size in the case of annealed sample and the boundaries between grains are very well defined (in comparison with sample 1), which could be attributed to the diffusion effect under high-temperature annealing. The inset figure presents the SAED pattern, showing that the grains are crystalline. The SAED pattern could be indexed perfectly with an α-alumina (PDF file 81-1667), and the rings are indexed as follows (from center to outer): (012), (104), (110), (006), (024), (116) and (214); the corresponding measured interplanar distances are: 3.50, 2.59, 2.40, 2.19, 1.77, 1.62 and 1.43 Å, respectively.

In order to study the interface between the adjacent grains we have performed HR-TEM measurements in the grain boundary. As can be seen in Figure 3a, the boundary is well defined in sample 1, whereas in sample 2 the boundaries are not clear. The inset figures show the fast Fourier transform of the selected zones. Figure 3a shows clearly the crystalline quality of the grains; we discern also a clear difference in orientation. In the case of annealed sample (Fig. 3b) we observe some diffusion between adjacent grains. Some reorganization in the interface of grains could be observed and results in a quasi-unique crystalline grain, which could be related to the high-temperature annealing effect.

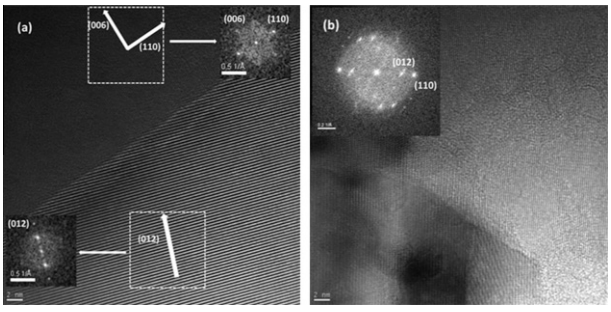

Figure 3. HR-TEM micrographs of (a) non-annealed sample and (b) annealed sample showing the crystallinity and the interface between grains before and after annealing.

In order to perform an in-depth structural characterization and to study the effect of annealing on both samples, a careful analysis of the HR-TEM images was made. Figure 4a shows a plan view HR-TEM micrograph of sample 1, where the presence of some linear fissures can be clearly observed. Figure 4b presents a Fourier-filtered image using (0 1 2); defects such as dislocations are clearly visible along the line fissure. It is worth noting that this type of fissure was not observed in sample 2.

In summary, the results presented in this paper demonstrate that SPS introduces residual strains in the material that must be taken into account because they affect the mechanical properties of the material. It also has been demonstrated that the presence of these strains can be easily removed by post-sintering thermal treatments. This is of crucial importance for the future design of materials with high mechanical properties and good creep behavior created using the non-conventional technique of fast SPS.

The authors would like to acknowledge the help of the EU for the financial support received under the IP-NANOKER NMP3-CT-2005-515784. A.B. acknowledges the Spanish Ministry of Science and Innovation for her Juan de la Cierva Contract (JCI-2011-10498). The authors are grateful to the Central Support Service in Experimental Research (SCSIE), University of Valencia for providing the HR-TEM facility.

[1] F. Wakai, S. Sagaguchi, Y. Matsuno, Adv. Ceram. Mater. 1 (1986) 259.
[2] F. Wakai, H. Kato, Adv. Ceram. Mater. 3 (1988) 71.
[3] K. Kajihara, Y. Yoshizawa, T. Sakuma, Acta Metall. Mater. 43 (1995) 1235.
[4] C.K. Yoon, I.W. Chen, J. Am. Ceram. Soc. 73 (1990) 1555.
[5] R.P. Dillon, S.S. Sosa, M.L. Mecartney, Scripta Mater. 50 (2004) 1441.

[6] B.N. Kim, K. Hiraga, K. Morita, Y. Sakka, Nature 413 (2001) 288.
[7] T. Chen, M.L. Mecartney, J. Am. Ceram. Soc. 88 (2005) 1004.
[8] L.A. Xue, I.W. Chen, J. Am. Ceram. Soc. 73 (1990) 2585.
[9] Z.J. Shen, M. Johnsson, Z. Zhao, M. Nygren, J. Am. Ceram. Soc. 85 (2002) 1921.
[10] L. Gao, H.Z. Wang, J.S. Hong, H. Miyamoto, K. Miyamoto, Y. Nishikawa, S.D.D.L. Torre, J. Eur. Ceram. Soc. 19 (1999) 609.
[11] L. Gao, J.S. Hong, H. Miyamoto, S.D.D.L. Torre, J. Eur. Ceram. Soc. 20 (2000) 2149.
[12] L. Gao, H. Wang, H. Kawaoka, T. Sekino, K. Niihara, J. Eur. Ceram. Soc. 22 (2002) 785.
[13] D. Sciti, F. Monteverde, S. Guicciardi, G. Pezzotti, A. Bellosi, Mater. Sci. Eng. A 434 (2006) 303.
[14] N. Tamari, I. Kondoh, T. Tanaka, N. Tokunaga, M. Kawahara, M. Tokita, K. Tezuka, T.J. Yamamoto, Ceram. Soc. Jpn. 105 (1997) 911.
[15] P. Miranzo, J.S. Moya, Ceram. Int. 10 (1984) 147.
[16] G.W. Hollenberg, G.R. Terwilliger, R.S. Gordon, J. Am. Ceram. Soc. 54 (1971) 196.
[17] H.P. Kirchner, R.M. Gruver, Mater. Sci. Eng. 13 (1974) 63.